Tunable wavelength hot electron light emitter

Article *in* Applied Physics Letters · September 1995

DOI: 10.1063/1.114700 · Source: IEEE Xplore

6 authors, including:

Ali Teke
Balikesir University
38 PUBLICATIONS **8,521** CITATIONS

Semicond. Sci. Technol. **12** (1997) 314–320. Printed in the UK PII: S0268-1242(97)78621-8

A tunable hot-electron light emitter

A Teke†, R Gupta‡, N Balkan‡, W van der Vleuten§ and J H Wolter§

† Department of Physics, Faculty of Art and Science, Balıkesir University, Balıkesir, Turkey
‡ Department of Physics, University of Essex, Colchester, CO4 3SQ, UK
§ Department of Physics, Eindhoven University of Technology, Eindhoven, The Netherlands

Received 11 October 1996, accepted for publication 19 November 1996

Abstract. We demonstrate the operation of a novel tunable wavelength surface emitting device. The device is based on a p-GaAs and n-$Ga_{1-x}Al_xAs$ heterojunction containing an inversion layer on the p-side, and GaAs quantum wells on the n-side, and is referred to as HELLISH-II (hot-electron light emitting and lasing in semiconductor heterojunction). The device utilizes hot-electron *longitudinal* transport and, therefore, light emission is independent of the polarity of the applied voltage. Because of this symmetric property, the device can perform light logic functions. The wavelength of the emitted light can be tuned with the applied bias from GaAs band-to-band transition in the inversion layer to e1–hh1 transition in the quantum wells. The operation of the device requires only two diffused in point contacts. Therefore, a two-dimensional array of surface emitters can be fabricated very cheaply and easily. Theoretical modelling of the device operation is carried out and compared with the experimental results. An optimized structure for high-efficiency device operation, as based on our model calculations, is also proposed.

1. Introduction

Research on simple devices that emit light from the surface which can be fabricated and tested easily as large-scale 2D arrays has been largely stimulated by potential applications in optical signal processing. These include light logic and optical computing, switching and interconnects. One possible candidate for such a device is HELLISH type I (hot-electron light emission and lasing in semiconductor heterojunction). This device has been proposed and studied extensively by us [1–3]. The main advantages of this device over conventional and quantum well light emitters are (i) only two diffused point contacts are needed so device fabrication is simple and cost effective and (ii) the light emission is due to carrier heating by the external bias, and, therefore, emitted light intensity is independent of the polarity of the applied voltage.

Another hot-electron light emitter, HELLISH type II, that also utilizes longitudinal transport and exhibits similar features to those of HELLISH-I has also been proposed by us [4, 5]. We have already demonstrated the operation of the device for single- and double-wavelength emission as tuned by the applied voltage. The aim of the current work is twofold: (i) to present the results for HELLISH-II for light logic operation up to three different wavelengths and (ii) to present our model calculations to optimize the operation of the device so as to enhance the emitted light intensity by about three orders of magnitude.

2. Experimental results

The structure and the schematic band diagram of the devices studied are shown in figure 1. The device coded as ES1 contains an inversion layer on the p-side and ten identical multiple quantum wells on the n-side of the p-GaAs–n-$Ga_{1-x}Al_xAs$ heterojunction. ES1 has been designed for single- and double-wavelength operation. The sample coded as ES6 has a structure similar to that of ES1. However, a set of two quantum wells with different well widths is incorporated away from the junction for triple-wavelength operation as will be discussed later. Both structures were grown using the MBE technique and fabricated into the form of simple bars. Ohmic contacts were made by diffusing Au–Ge–Ni to all the layers. Optical characterization of the devices was carried out using conventional photoluminescence (PL) techniques.

PL spectra of the samples measured at 77 K are shown in figures 2(a) and (b) for ES1 and ES6, respectively. In figure 2(a) the emission peak at $h\nu_2 = 1.58$ eV is the e1–hh1 emission for the $L_z = 75$ Å quantum wells. The broad peaks at lower energies correspond to the e–h recombination ($h\nu_1 = 1.52$ eV) and e–A^0 transition ($h\nu_0 = 1.49$ eV) in the inversion layer. In figure 2(b) the emission peaks at $h\nu_2' = 1.57$ eV and $h\nu_3' = 1.61$ eV are the e1–hh1 emissions of the $L_1 = 75$ Å and $L_2 = 50$ Å quantum wells, respectively. The peaks at $h\nu_1' = 1.52$ eV and $h\nu_0' = 1.50$ eV are the e–h and e–A^0 recombination in the inversion layer as in ES1, respectively.

0268-1242/97/030314+07$19.50

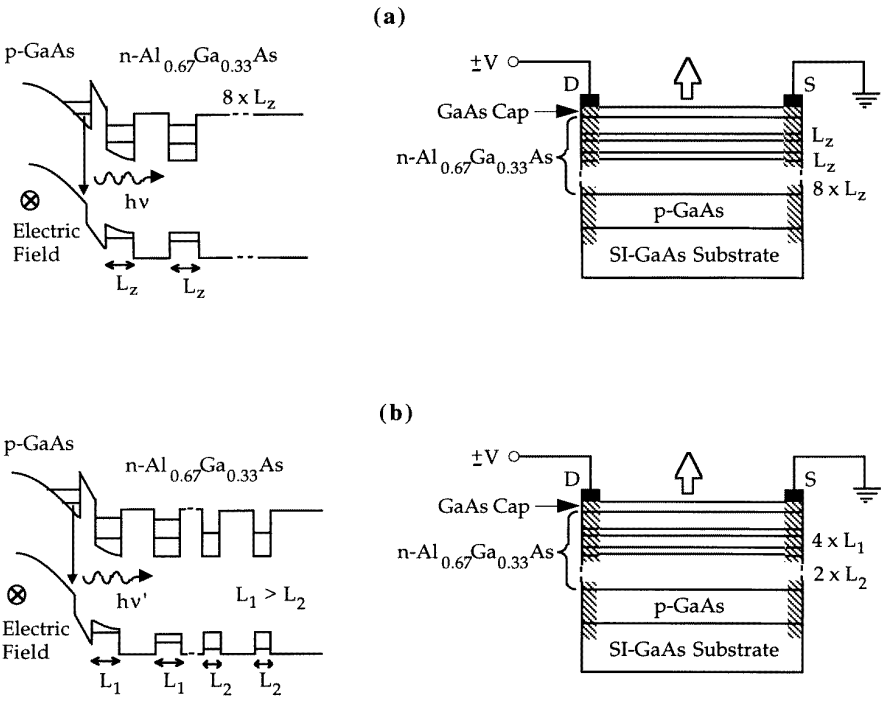

Figure 1. (a) The band structure and schematic diagram of the device coded as ES1 for single- and double-wavelength operation. L_z = 75 Å and L_B = 185 Å. The arrow indicates the emitted light. (b) The band structure and schematic diagram of the device coded as ES6 for single-, double- and triple-wavelength operation. L_1 = 75 Å, L_2 = 50 Å and L_B = 185 Å. The arrow indicates the emitted light.

Figure 3 shows the electroluminescence (EL) spectra of the samples for a number of different applied electric fields at 77 K. In these experiments electric field pulses of a few microseconds duration were applied along the layers with a duty cycle less than 0.1%. The EL was collected from the surface of the samples. The spectra were dispersed and recorded as described elsewhere [6]. The EL spectrum for ES1 has a single peak at $h\nu_1 = 1.52$ eV at low fields (figure 3(a)). When the electric field is increased, however, the spectrum develops a high-energy tail and the second peak at $h\nu_2 = 1.58$ eV, arising from the e1–hh1 transition for the $L_z = 75$ Å quantum wells, is observed. The intensity of the second peak grows faster than that of the first peak with the increasing field; eventually these two peak intensities become equal at an electric field around $F_{eq} = 1.2$ kV cm^{-1}. For ES6 the situation is almost the same (figure 3(b)). At low fields, EL spectra have two peaks at $h\nu_0' = 1.50$ eV and $h\nu_1' = 1.52$ eV (please note that the reason for having two well resolved peaks at the low-energy side of the EL spectra for sample ES6 compared with the single peak in sample ES1 has no significance, and is merely due to the difference in resolution of the experimental set-up). At higher fields the second $h\nu_2' = 1.58$ eV and third $h\nu_3' = 1.62$ eV peaks, which correspond to the e1–hh1 recombination in the first ($L_1 = 75$ Å) and the second ($L_2 = 50$ Å) quantum well, respectively, appear consecutively in EL spectra for sample ES6 (figure 3(b)). The peak intensities become equal at an electric field around $F_{eq} = 1.0$ kV cm^{-1}.

3. Theoretical modelling

To understand the device operation and optimize the structure, a physical model was applied to the system. The model involves the calculation of the potential profile of the device by using Schrödinger's and Poisson's equations self-consistently. Variational wave functions are used to describe the electrons in the inversion layer [7] and in the quantum well [8], and the Fermi level outside the depletion region is obtained from the 2D carrier concentration, which is measured experimentally. These calculations also yield the equilibrium electron concentrations in the well and in the inversion layer, n_w and n_{inv}, respectively. The calculated conduction band profile with the carrier dynamics involved in device operation is shown in figure 4. When the external field is applied parallel to the layers, the electrons in the quantum well are heated up; therefore, hot electrons in the quantum well adjacent to the junction plane are transferred to the inversion layer via phonon-assisted tunnelling and thermionic emission. In the case of the phonon-assisted tunnelling process, electrons are injected from the quantum well to the inversion layer by absorption of an optical phonon. Turley and Teitsworth [9] predicted that five different phonon modes play an important role in the phonon-assisted tunnelling current between the 2D states. In our case, the overlap integral I, involving the wavefunctions of electrons, in the well and in the inversion layer, with the displacement of the interface phonon, is expected to be small because of their very different z-dependences [5]. Therefore, we assumed that

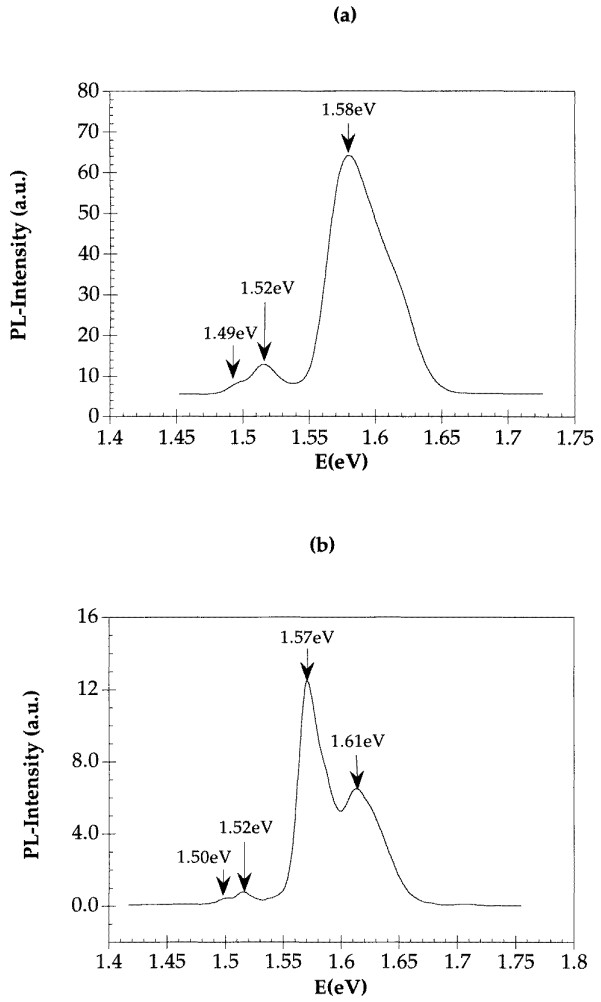

Figure 2. (a) The PL spectrum at T_L = 77 K for sample ES1. (b) The PL spectrum at T_L = 77 K for sample ES6.

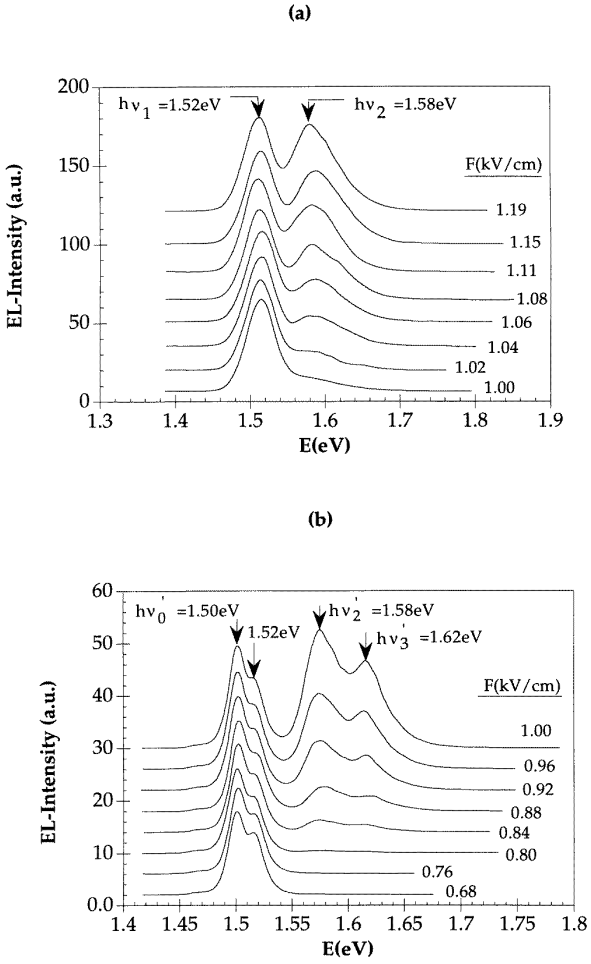

Figure 3. (a) EL spectra taken at T_L = 77 K for sample ES1. (b) EL spectra taken at T_L = 77 K for sample ES6.

the electron–(GaAs) confined phonon interaction [5], in the well, dominates over the other electron–phonon scattering processes. Thus, the temperature dependent tunnelling current density from quantum well to inversion layer is given by

$$J_{tun}(T_e) = \frac{e}{4\pi^3\overline{h}}\int [1 - f(\boldsymbol{k}'_{\parallel})]\,\mathrm{d}\boldsymbol{k}'_{\parallel} \times \int_{-\pi}^{\pi} \mathrm{d}\theta \int f(\boldsymbol{k}_{\parallel})\boldsymbol{k}_{\parallel}\,\mathrm{d}\boldsymbol{k}_{\parallel}\beta^2(\boldsymbol{q}_{\parallel})I^2(\boldsymbol{q}_{\parallel}) \times\delta(E_i - E_f + \overline{h}\omega) \quad (1)$$

where $f(\boldsymbol{k}_{\parallel})$ and $f(\boldsymbol{k}'_{\parallel})$ are the Fermi distribution function of electrons in the quantum well and in the inversion layer, respectively. i and f represent the initial and final electronic states, $\overline{h}\omega$ is the optical phonon energy and $\boldsymbol{k}_{\parallel}(\boldsymbol{k}'_{\parallel})$ and $\boldsymbol{q}_{\parallel}$ are electron and phonon wave vectors in the plane of the well (inversion layer) respectively. θ is the angle between the incoming, $\boldsymbol{k}_{\parallel}$, and the scattered, $\boldsymbol{k}'_{\parallel}$, electron. $\beta(\boldsymbol{q}_{\parallel})$ is the electron–phonon coupling constant and is given by

$$\beta^2(\boldsymbol{q}_{\parallel}) = \frac{\gamma_c^2}{L_z(q_{\parallel}^2 + k_z^2)} \quad (2)$$

where

$$\gamma_c = \left[\frac{\overline{h}\omega e^2}{\varepsilon_0}\left(\frac{1}{\kappa_\infty} - \frac{1}{\kappa_0}\right)\right]^{1/2} \qquad k_z = \alpha_n = \frac{n\pi}{L_z} \quad (3)$$

where κ_∞ and κ_0 are the high- and low-frequency dielectric constants, respectively. k_z is the electron wavevector perpendicular to the plane and L_z is the well width. Under the consideration of the assumption which has been made for the overlap integral $I(\boldsymbol{q}_{\parallel})$, the integration (1), in terms of energy over $\boldsymbol{k}_{\parallel}$ and θ, yields

$$J_{tun}(T_e) = \frac{em^*\gamma_c^2 I^2(\boldsymbol{q}_{\parallel})}{2\pi^2 L_z\overline{h}^3} \times \int_0^{\infty} \mathrm{d}E[\![\{\exp[(E' + \overline{h}\omega - \Delta E - E_{F_w})/k_B T_e] + 1\} \times\{\exp[(E_{F_{inv}} - E')/k_B T_e] + 1\}]\!]^{-1} \times \frac{1}{[2\overline{h}^2\alpha^2 E'/m^* + (\overline{h}^2\alpha^2/2m^* + \overline{h}\omega - \Delta E)^2]^{1/2}} \quad (4)$$

where E_{F_w} and $E_{F_{inv}}$ are the temperature dependent Fermi energies in the well and in the inversion layer with respect to the conduction band edge, respectively. ΔE is the energy difference between the confined states in the well and in the

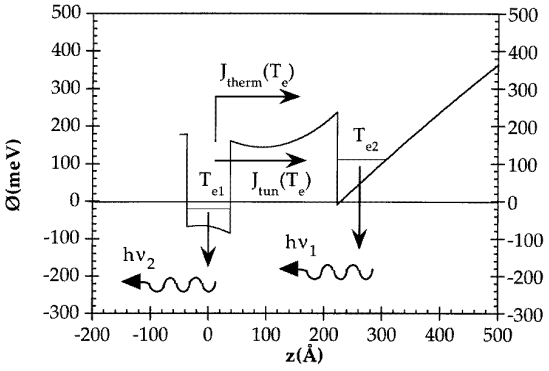

Figure 4. The calculated conduction band profile of the devices with a schematical illustration of the carrier dynamics involved in device operation. T_{e_1} and T_{e_2} are the electron temperatures in the quantum well and in the inversion layer, respectively. J_{therm} and J_{tun} are the thermionic and tunnelling components of the hot-electron currents. The light emissions are also indicated. Electric field is applied parallel to the layers.

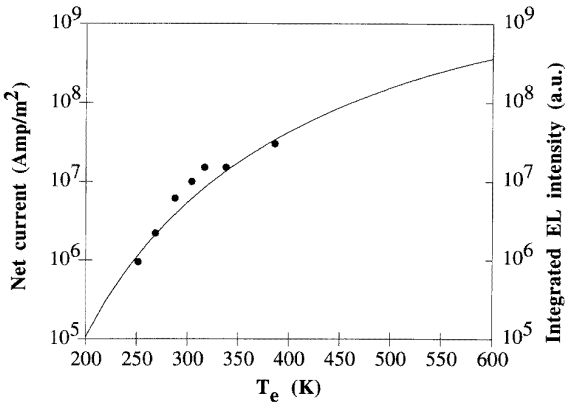

Figure 5. The temperature dependence of the calculated total hot-electron current from the quantum well to the inversion layer, J_{tot} (–), and the integrated EL intensity of the emitted light, I (●).

inversion layer. m^* is the electron effective mass, and $\overline{h}$ is the reduced Planck constant. The overlap integral, I, is

$$I = \int \Psi^*_{inv}(z)u(z)\Psi_w(z) \tag{5}$$

where Ψ_w and Ψ_{inv} are the unperturbated electron wave functions in the infinite-well approximation in the well and the inversion layer, and $u(z)$ is the phonon displacement which is given by $u(z) = \cos(\alpha_n z)$. In our calculations, the z-dependence of Ψ_{inv} is not available in the well. Therefore, we make the approximation

$$\Psi_{inv} = \sqrt{T_{wi}}\Psi_w \tag{6}$$

where T_{wi} is the tunnelling transmission co-efficient.

In the case of thermionic emission, electrons are transferred over the barrier from the quantum well to the inversion layer ballistically; therefore, we assumed that the transmission coefficient goes to unity. By applying the Maxwell–Boltzmann statistic with this assumption, the final form of thermionic emission current is given by [10]

$$J_{ther}(T_e) = \frac{em^*(k_B T_e)^2}{\pi^2 \overline{h}^3} \exp\left(\frac{E_F - V_b}{k_B T_e}\right) \tag{7}$$

where E_F is the Fermi energy and V_b is the barrier height between the quantum well and inversion layer in the conduction band. Other constants have their usual meanings. Although our quasi-static theoretical model does not include drift and diffusion processes for electrons and holes, or recombination dynamics, it gives a sufficiently good account of the device operation. Therefore it has been used to optimize the device structure for low-threshold-field and high-efficiency LED operation as will be discussed in the next section.

4. Discussion and conclusions

When the hot electrons in the quantum well adjacent to the junction plane are transferred to the inversion layer via phonon assisted tunnelling and thermionic emission as described above, the accumulation of excess negative charge in the inversion layer modifies the potential profile where the depletion region on the p-side of the junction is decreased so that the p-side of the depletion region behaves as if it were forward biased. The holes, therefore, which are initially away from the junction are injected towards the junction plane. Thus the electron and hole wave functions overlap in the vicinity of the inversion layer, giving rise to radiative recombination as observed in figure 3. As the field is increased the injected hot-electron current from quantum well to the inversion layer increases. Furthermore, the non-equilibrium electrons in the inversion layer (which also see the same external field) heat up and occupy the higher-energy states. Therefore, a high-energy tail which is representative of a Maxwellian distribution is expected to develop in the EL spectra as observed in figure 3(a). However, since the emitted light is collected from the surface of the samples, photons with energies $h\nu \geq h\nu_2$ are absorbed by the quantum well and re-emitted at energy $h\nu_2$ corresponding to the e1–hh1 transition in the well for ES1.

For ES6, however, not only are photons with energies $h\nu' \geq h\nu'_2$ absorbed by the first quantum well and re-emitted at energy $h\nu'_2$ corresponding to the e1–hh1 transition in the well ($L_1 = 75$ Å), but the re-emitted photons from the 75 Å quantum well with energies greater than e1–hh1 separation in the 50 Å well are absorbed and re-emitted by the 50 Å quantum well at energy $h\nu'_3$ corresponding to the e1–hh1 transition (figure 3(b)). With increasing field, both the injected hot-electron density in the inversion layer and the occupancy of high-energy states increases, so that more high-energy photons become available for absorption in the wells. As a result, the intensity of re-emission at $h\nu_2$ for sample ES1, and $h\nu'_2$ and $h\nu'_3$ for sample ES6, increases rapidly with increasing field as observed in figure 3.

Since we assumed that all the injected electrons recombine with holes, the temperature dependence of the

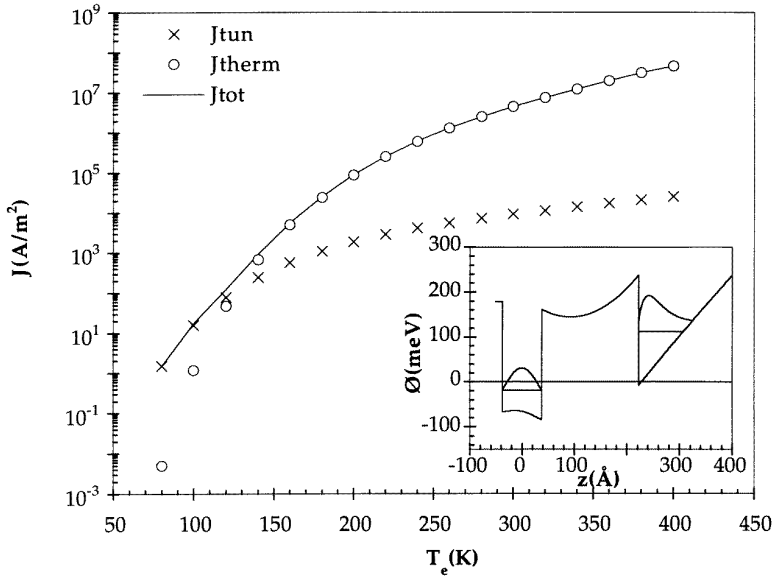

Figure 6. The temperature, T_e, dependence of the electronic currents, J_{tun}, J_{therm} and J_{tot}, from the quantum well to the inversion layer for ES1 with the parameters listed in table 1. Inset, the conduction band profile showing the electron wave functions in the well and in the inversion layer.

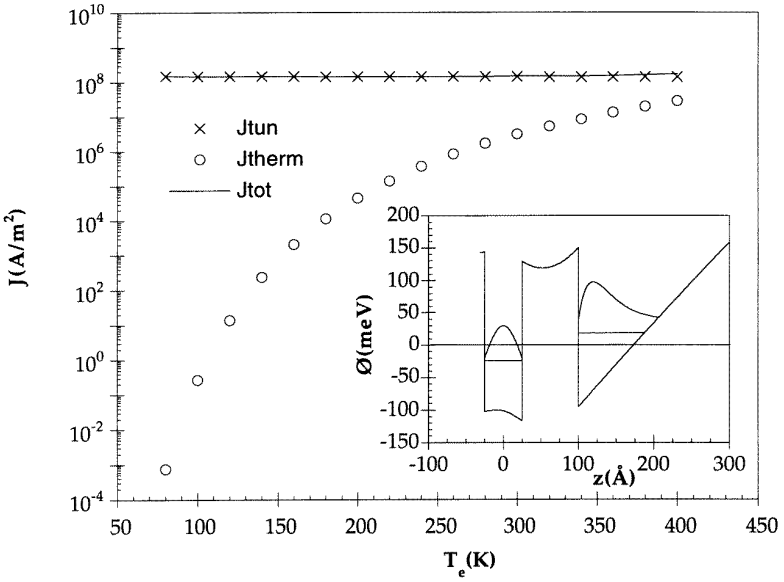

Figure 7. The temperature, T_e, dependence of the electronic currents, J_{tun}, J_{therm} and J_{tot}, from the quantum well to the inversion layer for the optimized device with the parameters listed in table 1. Inset, the conduction band profile showing the electron wave functions in the well and in the inversion layer.

current density should mimic that of the integrated EL intensity. This correlation is seen clearly in figure 5, where excellent agreement is achieved between the calculated temperature dependent hot-electron current density from quantum well to inversion layer and the experimentally obtained temperature dependent integrated EL intensity.

Device structure can be optimized for low-threshold and high-intensity output. This can be achieved by increasing the phonon assisted tunnelling current while the thermionic emission current is kept constant by changing structural parameters. For the devices ES1 and ES6 presented in this paper, the thermionic component of the total current dominates over the phonon assisted tunnelling one. This is due to the large potential barrier width and large energy separation of the quantum well and the inversion layer first subbands, $\Delta E = E_{1_{inv}} - E_{1_w}$, as indicated in figure 6. Two parameters play an important role in determining the phonon assisted tunnelling current in equation (4). The first one is the energy separation, ΔE, which should be close to the optical phonon energy $\hbar\omega$. The second one is

Table 1. Structural parameters of the optimized sample compared with those of sample ES1.

Sample parameters	ES1	Optimized structure
N_a (cm^{-3})	5.0×10^{16}	4.0×10^{16}
N_d (cm^{-3})	8.0×10^{17}	2.0×10^{18}
L_z (Å)	75	50
L_b (Å)	185	75
ΔE (meV)	131.73	43.17

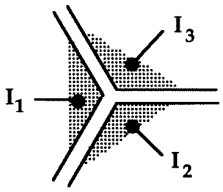

Figure 8. A schematic illustration of a three-input-terminal I_1, I_2 and I_3 device arranged with a threefold cyclic symmetry to perform the NAND and OR light logic functionally.

the barrier width, which should be reduced to increase the hot-electron tunnelling current from the quantum well to the inversion layer. We have calculated both the tunnelling and the thermionic current by choosing the optimized sample parameters as listed in table 1. The result is shown in figure 7. We obtain a tunnelling current far greater than both the thermionic and the tunnelling currents in sample ES1. We therefore expect enhanced emission from the optimized structure with less temperature dependence. Experimental work on the optimized device is currently underway and will be published very soon.

In conclusion, we have demonstrated the operation of a novel hot-electron surface light emitter, where the light emitted can be tuned from single- to multiple-wavelength operation by simply varying the applied voltage. The device, HELLISH-II, described here has may advantages over conventional light emitters. These are (i) the fabrication of the device is very simple, and only two diffused point contacts are required, (ii) light emission is due to carrier heating; the emitted light intensity is, therefore, independent of the polarity of the applied voltage, (iii) as a result of these two features the fabrication of a 2D array of surface emitters can be achieved easily and (iv) the devices can perform single- or multi-wavelength light logic tasks for a simple contact configuration with three input terminals. This is shown in figure 8 where I_1, I_2 and I_3 are arranged with a threefold cyclic symmetry and the truth chart for three-input operation is given in figure 9. In the table, V_1, V_2 and V_3 are the applied voltages for λ_1 emission only, λ_1 and λ_2 emissions, and λ_1, λ_2 and λ_3 emissions. If all the applied voltages are operative the light output shows NAND funciton. For a simple two-contact geometry the light output would be an exclusive OR function of the input polarity as demonstrated elsewhere [4]. Finally, in figure 10 we show the average emitted power from the surface of a (2.5×0.7 mm^2) device as a function of the

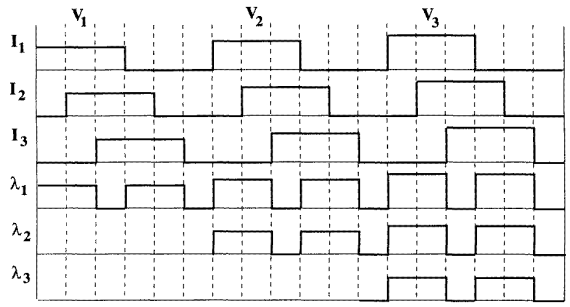

Figure 9. A schematic illustration of multi-wavelength, λ_1, λ_2 and λ_3, light logic functions for threefold cyclic symmetric input terminals, I_1, I_2 and I_3, at different applied voltages, V_1, V_2 and V_3, where $V_1 < V_2 < V_3$.

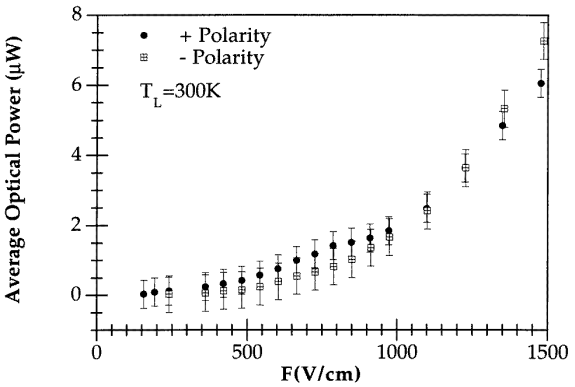

Figure 10. The average emitted power versus the applied electric field for both polarities in the sample ES1.

positive (+) and negative (-) applied voltage for the sample ES1. In order to enhance the light emission the device can easily be fabricated into a vertical cavity surface emitting laser (VCESL) device, by the inclusion of distributed Bragg reflectors (DBRs) at the top of the substrate and on top of the GaAs–AlGaAs quantum well structures as discussed in [11]. This work is under way and will be published in the near future.

Acknowledgments

We are grateful to EPSRC, UK, for financial support and to Balıkesir University, Turkey, for the PhD grant for A Teke.

References

[1] da Cunha A, Straw A and Balkan N 1993 *NDR and Instabilities in 2D Semiconductors* ed N Balkan, B K Ridley and A J Vickers (New York: Plenum) p 283
[2] da Cunha A, Gupta R, Straw A and Ridley B K 1994 *Semicond. Sci. Technol.* **9** 677
[3] Straw A, Balkan N, O'Brien A, da Cunha A, Gupta R and Arikan M C 1995 *Superlatt. Microstruct.* **18** 33
[4] Balkan N, Teke A, Gupta R, Straw A, Wolter J H and van der Vleuten W 1995 *Appl. Phys. Lett.* **67** 935
[5] Gupta R, Balkan N, Teke A, Straw A and da Cunha A 1995 *Superlatt. Microstruct.* **18** 45

[6] da Cunha A, Straw A, Gupta R, Balkan N and Ridley B K 1995 *J. Electrochem. Soc.* **94** 313
[7] Bastard G, Mendez E E, Chang L L and Esaki L 1983 *Phys. Rev.* B **28** 3241
[8] Ahn D and Chuang S L 1986 *Appl. Phys. Lett.* **49** 1450
[9] Turley P and Teitsworth S W *Phys. Rev.* B **50** 8423
[10] Straw A, da Cunha A, Gupta R, Balkan N and Ridley B K 1994 *Superlatt. Microstruct.* **16** 173
[11] Balkan N, da Cunha A, O'Brien A, Teke A, Gupta R, Straw A and Arikan M Ç 1996 *Hot Carriers in Semiconductors* ed K Hess *et al* (New York: Plenum) pp 603–9